J|A|C|S
ARTICLES

Spectroscopic and Density Functional Studies of the Red Copper Site in Nitrosocyanin: Role of the Protein in Determining Active Site Geometric and Electronic Structure

Lipika Basumallick,[†] Ritimukta Sarangi,[†] Serena DeBeer George,[‡] Brad Elmore,[§]
Alan B. Hooper,[*,§] Britt Hedman,[‡] Keith O. Hodgson,[†,‡] and Edward I. Solomon[*,†]

Contribution from the Department of Chemistry, Stanford University,
Stanford, California 94305, Stanford Synchrotron Radiation Laboratory,
Stanford Linear Accelerator Center, Stanford University, Stanford, California 94309,
and Department of Biochemistry, Molecular Biology and Biophysics,
University of Minnesota, St. Paul, Minnesota 55108

Received September 14, 2004; E-mail: edward.solomon@stanford.edu (E.I.S.); hooper@cbs.umn.edu (A.B.H.)

Abstract: The electronic structure of the red copper site in nitrosocyanin is defined relative to that of the well understood blue copper site of plastocyanin by using low-temperature absorption, circular dichroism, magnetic circular dichroism, resonance Raman, EPR and X-ray absorption spectroscopies, combined with DFT calculations. These studies indicate that the principal electronic structure change in the red copper site is the σ rather than the π donor interaction of the cysteine sulfur with the Cu 3d$_{x^2-y^2}$ redox active molecular orbital (RAMO). Further, MCD data show that there is an increase in ligand field strength due to an increase in coordination number, whereas resonance Raman spectra indicate a weaker Cu−S bond. The latter is supported by the S K-edge data, which demonstrate a less covalent thiolate interaction with the RAMO of nitrosocyanin at 20% relative to plastocyanin at 38%. EXAFS results give a longer Cu−S(Cys) bond distance in nitrosocyanin (2.28 Å) compared to plastocyanin (2.08 Å) and also show a large change in structure with reduction of the red copper site. The red copper site is the only presently known blue copper-related site with an exogenous water coordinated to the copper. Density functional calculations reproduce the experimental properties and are used to determine the specific protein structure contributions to exogenous ligand binding in red copper. The relative orientation of the CuNNS and the CuSC$_\beta$ planes (determined by the protein sequence) is found to be key in generating an exchangeable coordination position at the red copper active site. The exogenous water ligation at the red copper active site greatly increases the reorganization energy (by $\sim$1.0 eV) relative to that of the blue copper protein site, making the red site unfavorable for fast outer-sphere electron transfer, while providing an exchangeable coordination position for inner-sphere electron transfer.

1. Introduction

Blue copper centers are critical for intra- and inter-protein electron transfer in important biological processes of respiration, photosynthesis, nitrogen fixation, and lignin degradation.[1−7] The blue copper center found in plastocyanin, azurin, and related proteins has a Cu ion with an unusually short Cu−S(Cys) bond ($\sim$2.1 Å), two histidines with typical Cu−N(His) bonds ($\sim$2.0 Å), and a long axial Cu−S(Met) bond (2.8 Å) in a trigonally distorted tetrahedral geometry (Figure 1B).[8,9] The oxidized blue copper proteins exhibit an intense S(Cys) → Cu charge-transfer absorption band in the 600 nm region ($\epsilon \sim 5000$ M^{-1} cm^{-1}), resulting in their pronounced blue color. The electron paramagnetic resonance copper hyperfine splitting ($<|70| \times 10^{-4}$ cm^{-1}) is reduced to less than half the value observed for normal Cu(II) complexes ($>|150| \times 10^{-4}$ cm^{-1}). These unique spectral features have been attributed to a highly covalent Cu−S(Cys) interaction, with 38% S(Cys) 3p in the Cu 3d$_{x^2-y^2}$ orbital.[7,10] The key feature of the ground state is the strong π Cu−S(Cys) interaction, responsible for the characteristic blue copper absorption pattern, an intense low-energy π charge transfer (at $\sim$16,000 cm^{-1}) with a higher-energy weak σ charge transfer.

[†] Department of Chemistry, Stanford University.

[‡] Stanford Synchrotron Radiation Laboratory, Stanford University.

[§] University of Minnesota.

(1) Adman, E. T. In *Advances in Protein Chemistry*; Anfinsen, C. B., Richards, F. M., Edsall, J. T., Eisenberg, D. S., Eds.; Academic Press: San Diego, CA, 1991; Vol. 42, pp 145−198.

(2) Gray, H. B.; Solomon, E. I. *Copper Proteins*; Wiley: New York, 1981.

(3) Randall, D. W.; Gamelin, D. R.; LaCroix, L. B.; Solomon, E. I. *J. Biol. Inorg. Chem.* **2000**, *5*, 16−29.

(4) Solomon, E. I.; Baldwin, M. J.; Lowery, M. D. *Chem. Rev.* **1992**, *92*, 521−542.

(5) Solomon, E. I.; Lowery, M. D.; Guckert, J. A.; LaCroix, L. B. *Adv. Chem. Ser.* **1997**, *253*, 317−330.

(6) Solomon, E. I.; Randall, D. W.; Glaser, T. *Coord. Chem. Rev.* **2000**, *200−202*, 595−632.

(7) Solomon, E. I.; Szilagyi, R. K.; DeBeer George, S.; Basumallick, L. *Chem. Rev.* **2004**, *104*, 419.

(8) Colman, P. M.; Freeman, H. C.; Guss, J. M.; Murata, M.; Norris, V. A.; Ramshaw, J. A. M.; Venkatappa, M. P. *Nature* **1978**, *272*, 319−324.

(9) Guss, J. M.; Bartunik, H. D.; Freeman, H. C. *Acta Crystallogr.* **1992**, *B48*, 790−811.

(10) Shadle, S. E.; Penner-Hahn, J. E.; Schugar, H. J.; Hedman, B.; Hodgson, K. O.; Solomon, E. I. *J. Am. Chem. Soc.* **1993**, *115*, 767−776.

10.1021/ja044412+ CCC: $30.25 © 2005 American Chemical Society

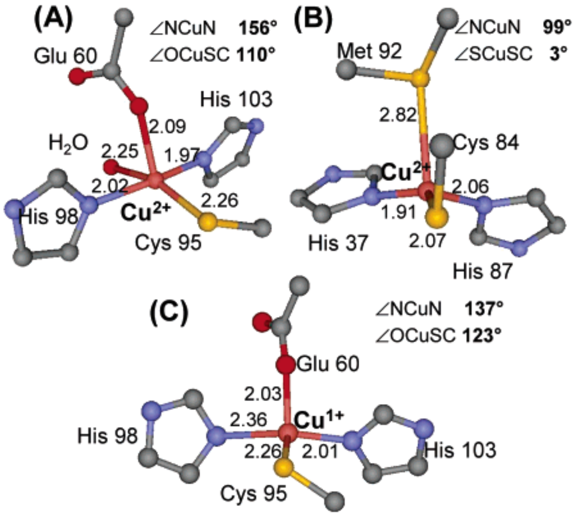

Figure 1. Crystal structures of (A) the oxidized red copper site in nitrosocyanin,[16] (B) the oxidized blue copper site in plastocyanin,[9] and (C) the reduced red copper site in nitrosocyanin.[16]

There are also a number of naturally occurring "perturbed" blue copper sites, which exhibit substantially different spectral features than those of classical blue sites.[11−15] They have the same ligand set but with shorter axial Cu−S(Met) and longer Cu−S(Cys) bonds (e.g., nitrite reductase Cu−S(Met) at 2.55 Å and Cu−S(Cys) at 2.16 Å, cucumber basic protein Cu−S(Met) at 2.61 Å and Cu−S(Cys) at 2.16 Å). When going from plastocyanin → cucumber basic blue → nitrite reductase (a green protein), the S(Cys) $\pi \rightarrow$ Cu 3d$_{x^2-y^2}$ charge-transfer intensity decreases while the S(Cys) $\sigma \rightarrow$ Cu 3d$_{x^2-y^2}$ charge-transfer intensity increases, indicating that the singly occupied 3d$_{x^2-y^2}$ acceptor orbital is rotated from a π to a σ bonding interaction with the S(thiolate) ligand. This dramatic spectral change is associated with a tetragonal distortion of the ligand field of the blue copper site in going to nitrite reductase. This short Cu−S(Met), long Cu−S(Cys), and tetragonal distortion has been referred to as the *coupled distortion*[14] and leads to the green color associated with the S(Cys) σ charge transfer.

Recently, a mononuclear red copper protein (nitrosocyanin) found in *Nitrosomonas europaea*, an ammonia oxidizing bacterium, was isolated and crystallographically characterized.[16,17] It exhibits significant sequence homology to blue copper proteins and has the characteristic Cu−thiolate bond. The 1.65 Å resolution crystal structure (Figure 1A) of the oxidized site shows that the copper ion is coordinated by two N(His), S(Cys), a side chain O of Glu, and has an additional fifth water ligand. The increased coordination due to the exogenous water ligand makes it a very distinct blue copper-related site. Nitrosocyanin has a strong absorption band at 390 nm (ϵ = 7000 M^{-1} cm^{-1}, resulting in its red color) and a reduction potential of 85 mV (lower than those of blue copper, which are in the range of 150−800 mV[7]). Studies on the reduced red copper site[16] indicate that it is four coordinate (Figure 1C), where the water molecule has been lost upon reduction. The biological role of this protein, however, has not been identified. It has been proposed that it might be involved in electron transfer or a catalytic function (due to the presence of the open coordination site).[16,17]

In this study, spectroscopic techniques, including low-temperature electronic absorption, circular dichroism, magnetic circular dichroism, electron paramagnetic resonance, resonance Raman, X-ray absorption edge, and EXAFS spectroscopies, have been complemented by spectroscopically calibrated density functional calculations to define the electronic structure of the red copper site. Geometric optimizations generate a detailed bonding description of the red copper center relative to the blue copper center and evaluate the role of the protein in exogenous ligand coordination to the Cu found only in this blue copper-related active site. The effect of this exogenous ligand binding on redox is considered.

2. Experimental Section

2.1. Samples. Red copper samples were purified from *Nitrosomonas europaea* as described previously.[16,17] Protein samples (∼0.5−1.5 mM, concentrated using Amicon or Microcon concentrators) were prepared as glasses in 50% (v/v) D_2O/glycerol-d_3 in 50 mM potassium phosphate buffer (pD* = 6.6). Samples were transferred to quartz EPR tubes, MCD cells, and XAS cells for spectroscopic characterization. Addition of glycerol had no effect on the CD spectra of the proteins. The Cu K-edge XAS data of both oxidized and reduced proteins were collected on frozen glass samples that contained 40−50% glycerol. The protein concentration (prior to glycerol addition) was ∼2.5 mM at pH 7 in HEPES buffer solution. All reduced Cu K-edge XAS samples were prepared by addition of 15-fold excess dithionite solution. Visual confirmation of reduction was the complete loss of the brilliant red color. S K-edge XAS data were collected on a ∼2 mM solution at pH 7 in phosphate buffer. The initial protein preparation used for S K-edge contained 1 equiv of adventitious Cu, which was not coordinated to the active site and hence did not affect pre-edge intensity; this however provided protein stability with respect to beam damage. The S K-edge data shown here were collected on this preparation. The integrity of the active site was confirmed by comparing the spectrum with data collected on a protein preparation from which the adventitious copper had been removed through EDTA treatment. Buffers were reagent grade and used without further purification. Water was purified to a resistivity of 15−18 MΩ with a Barnstead Nanopure deionizing system.

2.2. UV−Vis Electronic Absorption, Circular and Magnetic Circular Dichroism, and Electron Paramagnetic Resonance Spectroscopies. Absorption spectra at temperatures between 5 and 300 K were obtained using a computer-interfaced Cary-500 spectrophotometer modified to accommodate a Janis Research Super Vari-Temp cryogenic dewar mounted in the light path. Low-temperature circular dichroism and magnetic circular dichroism were performed using two Jasco spectropolarimeters. Each is equipped with a modified sample compartment to accommodate focusing optics and an Oxford Instruments SM4000-7T superconducting magnet/cryostat. This arrangement allows data collection at temperatures from 1.6 to 290 K and fields up to 7 T.[18] A Jasco J810 spectropolarimeter operating with a S-20 photomultiplier tube was used to access the visible and ultraviolet spectral region. A Jasco J200 spectropolarimeter operating with a liquid-nitrogen-cooled InSb detector was used for the near-infrared region. Special care was taken to provide magnetic shielding for the PMT detector. Depolar-

---

(11) Adman, E. T. *Topics in Molecular and Structural Biology: Metalloproteins*; Macmillan: New York, 1985; Vol. 1.

(12) Ellis, M. J.; Dodd, F. E.; Sawers, G.; Eady, R. R.; Hasnain, S. S. *J. Mol. Biol.* **2003**, *328*, 429−438.

(13) Lu, Y.; LaCroix, L. B.; Lowery, M. D.; Solomon, E. I.; Bender, C. J.; Peisach, J.; Roe, J. A.; Gralla, E. B.; Valentine, J. S. *J. Am. Chem. Soc.* **1993**, *115*, 5907−5918.

(14) LaCroix, L. B.; Shadle, S. E.; Wang, Y. N.; Averill, B. A.; Hedman, B.; Hodgson, K. O.; Solomon, E. I. *J. Am. Chem. Soc.* **1996**, *118*, 7755−7768.

(15) LaCroix, L. B.; Randall, D. W.; Nersissian, A. M.; Hoitink, C. W. G.; Canters, G. W.; Valentine, J. S.; Solomon, E. I. *J. Am. Chem. Soc.* **1998**, *120*, 9621−9631.

(16) Lieberman, R. L.; Arciero, D. M.; Hooper, A. B.; Rosenzweig, A. C. *Biochemistry* **2001**, *40*, 5674−5681.

(17) Arciero, D. M.; Pierce, B. S.; Hendrich, M. P.; Hooper, A. B. *Biochemistry* **2002**, *41*, 1703−1709.

ization of the light by the MCD samples was monitored by their effect on the CD signal of nickel (+)-tartarate placed before and after the sample. In all cases, the depolarization was less than 5%.[19] CD samples were run in a 1.0 cm quartz cuvette. MCD samples were run in cells fitted with quartz disks and a 0.3 cm rubber gasket spacer. Simultaneous Gaussian fitting of the low-temperature absorption, MCD, and CD spectra was performed using the Peak-Fit program (Jandel). EPR spectra were obtained using a Bruker EMX spectrometer. All samples were run at 77 K in a liquid nitrogen finger dewar. Spin quantitation of the EPR spectra was accomplished using $Cu(ClO_4)_2$[20] as a standard. Simulations of EPR spectra were performed using the program XSophe.[21]

2.3. Resonance Raman Spectroscopy. Resonance Raman spectra were collected with a Princeton Instruments ST-135 back-illuminated CCD detector on a Spex 1877 CP triple monochromator with 1200, 1800, and 2400 grooves/mm holographic spectrograph gratings. Continuous-wave Coherent Kr ion (Innova90C-K) and an Ar ion (Sabre-25/7) visible and UV laser lines were used as variable excitation sources. A polarization scrambler was used between the sample and the spectrometer. The Raman energy was calibrated with Na_2SO_4. Frequencies are accurate to <2 cm^{-1}. Samples were loaded in 4 mm NMR tubes and stored in liquid nitrogen.

2.4. X-ray Absorption Spectroscopy. 2.4.1. Cu K-Edge. The Cu K-edge X-ray absorption spectroscopy data were measured at the Stanford Synchrotron Radiation Laboratory on the unfocused 8-pole, 1.8 T wiggler beam line 7-3 under standard ring conditions of 3 GeV and 60−100 mA. A Si(220) double crystal monochromator was used for energy selection and detuned by 50% to minimize higher harmonic components in the X-ray beam. The protein solutions were loaded into 1 mm Lucite XAS cells with X-ray transparent ~37 μm Kapton windows. The samples were immediately frozen thereafter and stored under liquid nitrogen conditions. The samples were maintained at a constant temperature of ~10 K during data collection using an Oxford Instruments CF1208 continuous flow liquid helium cryostat. Data were measured up to $k = 16$ Å^{-1} in fluorescence mode using a Canberra Ge 18-element array detector, which was possible since there was no adventitious zinc contamination in the protein. Internal energy calibration was accomplished by simultaneous measurement of the absorption of a Cu foil placed between two ionization chambers situated after the sample. The first inflection point of the foil spectrum was assigned to 8980.3 eV. Due to photoreduction of the oxidized protein, a total of four spots on two sample cells were used for data collection and analysis. Four scans could be collected on each spot before the effect of photoreduction was observed (as an energy shift in the rising edge). A total of 11 scans were used for the oxidized form, whereas a total of 20 scans were measured and averaged for the reduced protein sample.

The energy-calibrated data were averaged and processed by fitting a second-order polynomial to the pre-edge region, which was subtracted from the entire spectrum as background. A three-region spline of orders 2, 3, and 3 was used to model the post-edge region background. Normalization of the data was achieved by subtracting the cubic spline and assigning the edge jump to 1.0 at 9000 eV using the *SPLINE* routine in the XFIT suite of programs.[22] Theoretical EXAFS signals, $\chi(k)$, were calculated using *FEFF* (version 7.0),[23,24] and structural models derived from the crystal structures of the oxidized and reduced protein were fit to the data using EXAFSPAK.[25] The experimental threshold energy, E_0, was chosen as 9000 eV. The structural parameters varied during the fitting process include the bond distance (R) and the bond variance (σ^2), which is related to the Debye−Waller factor, resulting from thermal motion and static disorder of the absorber−scatter pair. The nonstructural parameter, ΔE_0, was also allowed to vary but was restricted to a common value for every component in a given fit. Coordination numbers were systematically varied in the course of the fitting process but were fixed within a given fit.

2.4.2. S K-Edge. S K-edge data of the oxidized protein were measured using the 54-pole wiggler beam line 6-2 in high magnetic field mode of 10 kG with a Ni-coated harmonic rejection mirror and a fully tuned Si(111) double crystal monochromator. Details of the optimization of this beam line for low-energy measurements and the experimental setup have been described in an earlier publication.[26] The protein solution was pre-equilibrated in a water-saturated He atmosphere for ~1 h to minimize He bubble formation in the sample cell during the experiment. Protein solutions were loaded into a Pt-coated Al-block sample holder with a ~6.35 μm thick polypropylene window using a syringe. S K-edge measurements were performed at ~4 °C. The temperature was regulated using a cryostat, which utilizes liquid-nitrogen-cooled N_2 gas flowing through an internal channel in the sample holder. Sulfur fluorescence data were collected using a N_2-filled ionization chamber as a detector.[27,28] The protein samples were monitored for potential effects of photoreduction through the course of data collection, and 10-fold excess of $K_3[Fe(CN)_6]$ in phosphate buffer was added to oxidize the partially reduced protein to acquire a total of nine scans.

The S K-edge data presented here were averaged and processed as described in an earlier publication.[26] Energy calibration was achieved from the S K-edge spectra of $Na_2S_2O_3 \cdot 5H_2O$ run at intervals between sample scans. The first inflection point was assigned to 2472.02 eV. A sharp sulfate feature was observed at ~2482.4 eV, which was present due to the use of ammonium sulfate during protein purification. S K-edge data were therefore measured for Na_2SO_4 in solution. A smooth polynomial background of order 2 was fit to the pre-edge and subtracted from the entire energy range of each data set. Normalization was achieved by fitting a linear polynomial to the post-edge and normalizing the edge jump to 1 at 2540 eV; 26% of the normalized sulfate spectrum was then subtracted from the normalized sample spectrum to completely eliminate the sulfate peak at ~2482.4 eV in the sample spectrum, and the resulting sample spectrum was renormalized to 1 at 2540 eV. The area under the pre-edge peak was quantified by fitting the data using EDG_FIT.[25] The pre-edge and rising-edge features were modeled with pseudo-Voigt line-shapes with a fixed 1:1 Lorentzian:Gaussian ratio. The reported intensity and half-width value are based on an average over simultaneous fits that accurately modeled the data and the second derivative. Normalization procedures introduce ~3% error in the value of the integrated area under the pre-edge peak.

2.5. Electronic Structure Calculations. Gradient-corrected density functional calculations (GGA-DFT) were carried out using the Gaussian98[29] package on a 80 cpu heterogeneous cluster of SGI and IBM PC-compatible computers. The Becke88[30] exchange and Perdew86[31]

---

(18) Allendorf, M. D.; Spira, D. J.; Solomon, E. I. *Proc. Natl. Acad. Sci. U.S.A.* **1985**, *82*, 3063−3067.
(19) Browett, W. R.; Fucaloro, A. F.; Morgan, T. V.; Stephens, P. J. *J. Am. Chem. Soc.* **1983**, *105*, 1868−1872.
(20) Carithers, R. P.; Palmer, G. *J. Biol. Chem.* **1981**, *256*, 7967−7976.
(21) Wang, D. M.; Hanson, G. R. *J. Magn. Reson.* **1995**, *117*, 1−8.
(22) Ellis, P. J.; Freeman, H. C. *J. Synchrotron Radiat.* **1995**, *2*, 190−195.
(23) Deleon, J. M.; Rehr, J. J.; Zabinsky, S. I.; Albers, R. C. *Phys. Rev. B* **1991**, *44*, 4146−4156.
(24) Rehr, J. J.; Deleon, J. M.; Zabinsky, S. I.; Albers, R. C. *J. Am. Chem. Soc.* **1991**, *113*, 5135−5140.
(25) George, G. N. *EXAFSPAK & EDG_FIT*; Stanford Synchrotron Radiation Laboratory, 2000.
(26) Hedman, B.; Frank, P.; Gheller, S. F.; Roe, A. L.; Newton, W. E.; Hodgson, K. O. *J. Am. Chem. Soc.* **1988**, *110*, 3798−3805.
(27) Lytle, F. W.; Greegor, R. B.; Sandstrom, D. R.; Marques, E. C.; Wong, J.; Spiro, C. L.; Huffman, G. P.; Huggins, F. E. *Nucl. Instrum. Methods Phys. Res., Sect. A* **1984**, *226*, 542−548.
(28) Stern, E. A.; Heald, S. M. *Rev. Sci. Instrum.* **1979**, *50*, 1579−1582.
(29) Frisch, M. J.; Trucks, G. W.; Schlegel, H. B.; Scuseria, G. E.; Robb, M. A.; Cheeseman, J. R.; Zakrzewski, V. G.; Montgomery, J. A., Jr.; Stratmann, R. E.; Burant, J. C.; Dapprich, S.; Millam, J. M.; Daniels, A. D.; Kudin, K. N.; Strain, M. C.; Farkas, O.; Tomasi, J.; Barone, V.; Cossi, M.; Cammi, R.; Mennucci, B.; Pomelli, C.; Adamo, C.; Clifford, S.; Ochterski, J.; Petersson, G. A.; Ayala, P. Y.; Cui, Q.; Morokuma, K.; Malick, D. K.; Rabuck, A. D.; Raghavachari, K.; Foresman, J. B.; Cioslowski, J.; Ortiz, J. V.; Stefanov, B. B.; Liu, G.; Liashenko, A.; Piskorz, P.; Komaromi, I.; Gomperts, R.; Martin, R. L.; Fox, D. J.; Keith, T.; Al-Laham, M. A.; Peng, C. Y.; Nanayakkara, A.; Gonzalez, C.; Challacombe, M.; Gill, P. M. W.; Johnson, B.; Chen, W.; Wong, M. W.; Andres, J. L.; Head-Gordon, M.; Replogle, E. S.; Pople, J. A.; *Gaussian98*, revision A.1; Gaussian, Inc.: Pittsburgh, PA, 1998.

correlation nonlocal functionals were used with Wosko−Vilk−Nusair[32] local functionals as implemented in the software package (BP86). The triple-ζ (VTZ*)[33] and double-ζ (6-31G*)[34−36] Gaussian-type all-electron basis sets (BS5) were employed with polarization functions for the metal and ligand atoms, respectively. These basis sets have been previously shown to be theoretically converged for Cu(II)-containing systems, and additional polarization or diffuse functions do not improve the electronic structure description.[37−39] Since standard GGA-DFT calculations result in too much ligand character in the ground-state wave function compared to that in experiment, 38% of total DF exchange was replaced with HF exchange (B(38HF)P86), giving a more accurate bonding description, as discussed for other cupric systems.[39] Population analyses were performed by means of Weinhold's Natural Population Analysis (NPA),[40−42] including the Cu 4p orbitals in the valence set. Wave functions were visualized in Molden. Compositions of molecular orbitals and overlap populations between molecular fragments were calculated using the AOMix[43,44] program. The electronic absorption spectrum was calculated with time-dependent density functional theory (TD-DFT) using Gaussian 98. The energies and intensities of the lowest 40 transitions were calculated with TD-DFT. The absorption profile was obtained using the SWizard[45] program (version 3.6). The total integrated intensity under the absorption profile is equal to the sum of the oscillator strengths. The half-bandwidths were assumed to be equal to 3000 cm^{-1} (a typical half-bandwidth for electronic transitions in transition metal sites). DFT calculations (including ΔSCF) were also performed with the Amsterdam Density Functional program package (ADF 2003.01).[46−48] An uncontracted, all-electron triple-ζ basis set with a single polarization function (TZP) was employed. Convergence was reached when the maximum element in the error matrix was $<10^{-5}$. Orbitals were plotted using gOpenMol.[49]

Geometry optimizations were performed with frequent updates of the force constants in order to stay as close as possible to the lowest-energy pathway. Stationary points were restarted with continuous update of force constants until the optimization terminated due to negligible forces. In all optimizations, the GDIIS[50−52] optimizer was applied due to the flat potential energy surface of the Cu site. The protein pocket was simulated by keeping the relative distance of the α carbons of the ligands bound to copper fixed during geometry optimizations.

The computational models of the active sites were constructed from imidazole, methyl thiolate, acetate, and water molecules. The starting atomic coordinates for geometry optimizations of the oxidized (1.65 Å resolution) and reduced (2.3 Å resolution) red copper active site geometries were taken from the X-ray structures[16] of the nitrosocyanin (*Nitrosomonas europaea*). Geometry optimizations were also performed on a model derived from the EXAFS best fit parameters of the oxidized red copper active site.

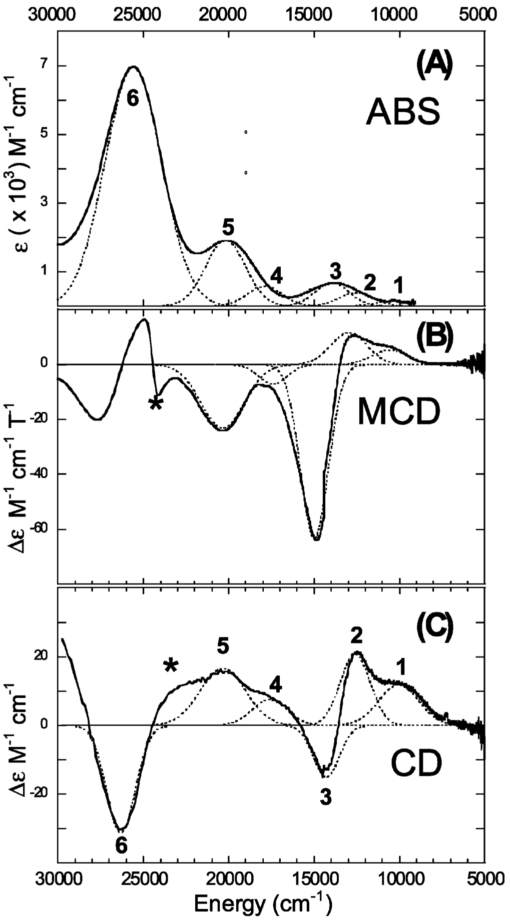

Figure 2. Electronic absorption (A), magnetic circular dichroism (B), and circular dichroism (C) spectra of nitrosocyanin. Abs, MCD, and CD spectra were obtained at 5 K, and samples were prepared as glasses in 50% (v/v) glycerol-d_3 in 50 mM phosphate (pD* = 6.6). The dotted lines represent the individual Gaussian bands obtained by a simultaneous least-squares fit of the Abs, MCD, and CD data. The derivative-shaped MCD feature at 24,000 cm^{-1} (marked as ∗) is due to a small amount of heme present in the protein sample.

3. Results

3.1. Absorption/CD/MCD/EPR. Low-temperature absorption, CD, and MCD spectra between 5000 and 30,000 cm^{-1} for nitrosocyanin are presented in Figure 2. Simultaneous Gaussian resolution requires six bands to adequately fit the spectra and have been depicted by the dashed lines in the three panels. Energies, ϵ, and $\Delta\epsilon$ values for the bands determined from these fits are summarized in Table 1. In the low-energy region ($<$20,000 cm^{-1}), four bands are observed at 10,500 cm^{-1} (band 1), 12,900 cm^{-1} (band 2), 15,000 cm^{-1} (band 3), and 17,600 cm^{-1} (band 4). Two intense (in absorption) transitions (bands 5 and 6) contribute to the absorption intensity at 20,350 and 25,550 cm^{-1}, respectively. No transitions are present in the 5000−10,000 cm^{-1} region.

Bands can be differentiated as ligand field and charge transfer from their relative intensities in MCD and absorption spectra. The parameter used is the ratio of C_0, the MCD C-term intensity, and D_0, the dipole strength in absorption. C_0/D_0 ratios were

---

(30) Becke, A. D. *Phys. Rev. A* **1988**, *38*, 3098−3100.
(31) Perdew, J. P. *Phys. Rev. B* **1986**, *33*, 8822−8824.
(32) Vosko, S. H.; Wilk, L.; Nusair, M. *Can. J. Phys.* **1980**, *58*, 1200−1211.
(33) Schaefer, A.; Horn, H.; Ahlrichs, R. *J. Chem. Phys.* **1992**, *97*, 2571−2577.
(34) Hariharan, P. C.; Pople, J. A. *Theor. Chim. Acta* **1973**, *28*, 213−222.
(35) Francl, M. M.; Hehre, W. J.; Binkley, J. S.; Gordon, M. S.; DeFrees, D. J.; Pople, J. A. *J. Chem. Phys.* **1982**, *77*, 3645−3665.
(36) Rassolov, V. A.; Pople, J. A.; Ratner, M. A.; Windus, T. L. *J. Chem. Phys.* **1998**, *109*, 1223−1229.
(37) Siegbahn, P. E.; Blomberg, M. R. A. *Chem. Rev.* **2000**, *100*, 421−437.
(38) Ryde, U.; Olsson, M. H. M.; Pierloot, K. *Theor. Comput. Chem.* **2001**, *9*, 1−55.
(39) Szilagyi, R. K.; Metz, M.; Solomon, E. I. *J. Chem. Phys.* **2002**, *106*, 2994−3007.
(40) Foster, J. P.; Weinhold, F. *J. Am. Chem. Soc.* **1980**, *102*, 7211−7218.
(41) Reed, A. E.; Curtiss, L. A.; Weinhold, F. *Chem. Rev.* **1988**, *88*, 899−926.
(42) Carpenter, J. E.; Weinhold, F. *THEOCHEM* **1988**, *169*, 41−62.
(43) Gorelsky, S. I. *AOMix Program*, revision 5.9, http://www.sg-chem.net/.
(44) Gorelsky, S. I.; Lever, A. B. P. *J. Organomet. Chem.* **2001**, *635*, 187−196.
(45) Gorelsky, S. I. *SWizard Program*, http://www.sg-chem.net/.
(46) *ADF2003.01 SCM*; Theoretical Chemistry, Vrije Universiteit: Amsterdam, The Netherlands, http://www.scm.com.
(47) Fonseca Guerra, C.; Snijders, J. G.; te Velde, G.; Baerends, E. J. *Theor. Chem. Acc.* **1998**, *99*, 391−403.
(48) te Velde, G.; Bickelhaupt, F. M.; van Gisbergen, S. J. A.; Fonseca Guerra, C.; Baerends, E. J.; Snijders, J. G.; Ziegler, T. *J. Comput. Chem.* **2001**, *22*, 931−967.
(49) *gOpenMol CSC*, http://www.csc.fi/goopenmol/.
(50) Csaszar, P.; Pulay, P. *J. Mol. Struct. (THEOCHEM)* **1984**, *114*, 31−34.
(51) Farkas, O.; Schlegel, H. B. *J. Chem. Phys.* **1998**, *109*, 7100−7104.
(52) Farkas, O.; Schlegel, H. B. *J. Chem. Phys.* **1999**, *111*, 10806−10814.

Table 1. Experimental Spectroscopic Parameters for Nitrosocyanin

band	assignment	energy (cm^{-1})	ϵ (M^{-1} cm^{-1})	$\Delta\epsilon$ (M^{-1} cm^{-1} T^{-1})	C_0/D_0
1	d_{xz}	10500	430[b]	+5	0.1
2	d_{yz}	12900	540	+12	0.16
3	d_{z^2}	15000	810	−60	0.5
4	d_{xy}	17600[a]	650	−7	0.1
5	Cys π	20350	2200	−20	0.06
6	Cys σ	25550	7000	−21	0.02

[a] Position of band 4 determined from MCD and CD data. [b] Upper ϵ limit in absorption.

determined from the Gaussian fit of the MCD data taken within the linear $1/T$ region and the absorption spectra[53] using the relation

$$C_0/D_0 = (kT\Delta\epsilon)/(\mu_B B\epsilon_{max})$$

where T is the temperature, B the external magnetic field strength, k the Boltzmann constant, μ_B the Bohr magneton, ϵ_{max} the absorption maximum in M^{-1} cm^{-1}, and $\Delta\epsilon$ the MCD intensity maximum measured in M^{-1} cm^{-1} ($k/\mu_B \approx 1.489$ TK^{-1}). C-term MCD intensity of paramagnetic systems depends on the spin−orbit coupling for the center involved in the transition.[54] The spin−orbit coupling for Cu is greater than that for S, N, and O (ξ(Cu) = 830 cm^{-1}, ξ(S) = 382 cm^{-1}, ξ(N) = 70 cm^{-1}, and ξ(O) = 70 cm^{-1}). This makes the C_0/D_0 ratio sensitive to the amount of metal character in the excited states. Transitions centered on Cu (i.e., d → d) have C_0/D_0 ratios higher than those of charge-transfer transitions that involve significant S or N character. Alternatively, absorption intensity is proportional to ligand−ligand overlap and is greater for the two levels involved in a charge-transfer transition.

The four lower-energy bands (bands 1−4; see Table 1) in nitrosocyanin can be assigned as ligand field transitions as they exhibit the largest $|C_0/D_0|$ ratios ($\geq$0.1) and are weak in absorption. The ligand field transitions in the red copper site, which cover the region 10,500−17,600 cm^{-1}, are shifted to higher energy relative to those of typical blue (e.g., plastocyanin[54,55]) and green copper (e.g., nitrite reductase[14]) sites, which range from 5000 to 14,000 cm^{-1}. The specific assignment of d → d transitions are made in section 4.1.3 on the basis of the magnitude and MCD sign of the observed bands.

The higher-energy transitions (bands 5 and 6) have high absorption intensity ($\epsilon \sim 2200$ and 7000 M^{-1} cm^{-1}) and relatively low MCD intensity ($|\Delta\epsilon| = 20$ and 21 M^{-1} cm^{-1} T^{-1}, respectively), giving $|C_0/D_0| < 0.06$, and are assigned as S(Cys)-to-Cu charge-transfer transitions (from resonance Raman, vide infra). Band 5 is the lowest-energy charge-transfer transition and is assigned as the S(Cys) $\pi \rightarrow$ Cu $d_{x^2-y^2}$ charge-transfer transition. Note that EPR ($g_{||} > g_{\perp} > 2.0023$)[17] and density functional calculations (section 4) identify $d_{x^2-y^2}$ as the highest-energy singly occupied molecular orbital (which is the RAMO). The higher-energy intense absorption (band 6) is assigned to the S(Cys) pseudo $\sigma \rightarrow$ Cu $d_{x^2-y^2}$ charge-transfer transition. It is responsible for the intense red color of this protein. The cysteine-to-copper charge-transfer transitions are shifted to higher energies in red copper in comparison to those of blue (by 5250 cm^{-1}) and green (by 3250 cm^{-1}) copper centers. Additionally, the intensity ratio (S(Cys) pseudo σ/S(Cys) $\pi > 3$) is unique to the red copper site. In a blue copper site (e.g., plastocyanin), the σ/π ratio = 0.1,[54,55] and in a green copper site (e.g., nitrite reductase), the intensity ratio is 2.[14] The charge-transfer region of the red copper site is thus dramatically different from that in the blue and green copper sites.

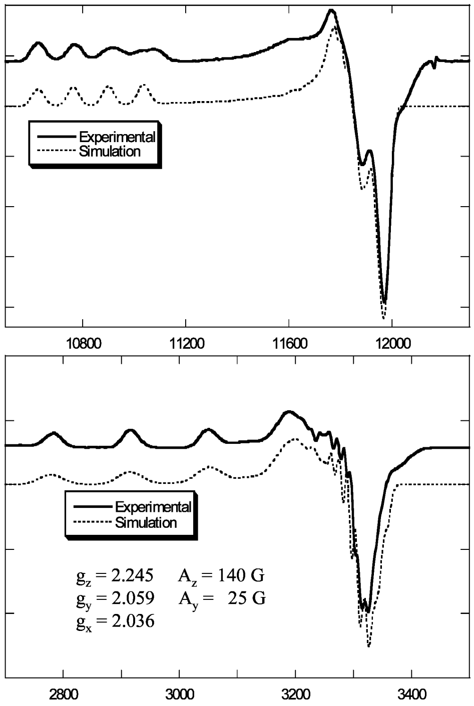

Figure 3. Q-band (top) and X-band (bottom) EPR data (—) and simulations (- - -) of nitrosocyanin in 50 mM potassium phosphate (pH = 7.0). The parameters used for the simulations are given in the bottom spectra. The instrumental conditions were as follows: Q-band −77 K, frequency 34.09 GHz, microwave power 0.416 mW; X-band −77 K, frequency 9.37 GHz, microwave power 10 mM.

Figure 3 shows the Q- and X-band EPR spectra and simulations for nitrosocyanin. The combination of Q- and X-band EPR provides accurate g values, which are similar to those determined in a previous study.[17] The spin Hamiltonian parameters of the XSophe[21] simulations are given in the lower panel. Two equivalent nitrogen atoms ($I = 1$) for the two N(His) ligands with isotropic A values (14×10^{-4} cm^{-1}) were included in the fit. The observed g values ($g_{||} > g_{\perp} > 2.0023$) are consistent with a $d_{x^2-y^2}$ highest-energy half-occupied molecular orbital. The g values and hyperfine constants provide additional insight into the electronic structure of the red copper center (see section 4.2.2).

No pH effect is observed for nitrosocyanin using glutamate buffer and the "universal buffer" between pH 4 and 10. This indicates that the exogenous ligand in the red copper site is water rather than hydroxide over this pH range.

3.2. Resonance Raman. Figure 4 presents the resonance Raman spectra of nitrosocyanin with excitation energy at 407 and 502 nm into the S(Cys) → Cu pseudo σ (band 6) and π (band 5) charge-transfer bands, respectively. The red copper site displays an envelope of resonance Raman peaks between 300 and 350 cm^{-1}, associated with vibrations containing the Cu−S distortion. The envelope is due to coupling of the Cu−S

---

(53) Piepho, S. B.; Schatz, P. N. *Group Theory in Spectroscopy: With Applications to Magnetic Circular Dichroism*; John Wiley & Sons: New York, 1983.

(54) Gewirth, A. A.; Solomon, E. I. *J. Am. Chem. Soc.* **1988**, *110*, 3811−3819.

(55) Penfield, K. W.; Gay, R. R.; Himmelwright, R. S.; Eickman, N. C.; Freeman, H. C.; Solomon, E. I. *J. Am. Chem. Soc.* **1981**, *103*, 4382−4388.

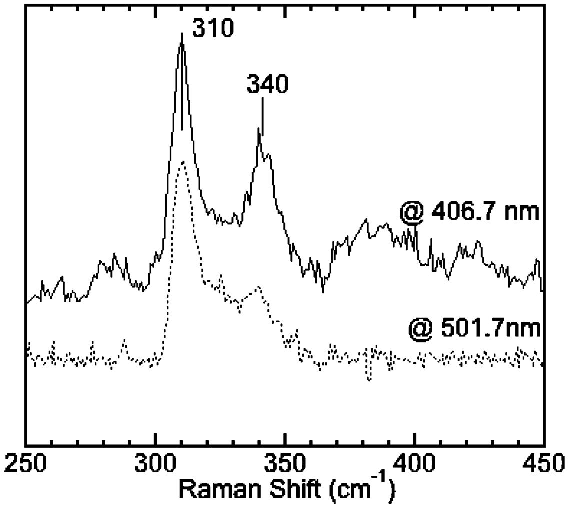

Figure 4. Resonance Raman spectra of nitrosocyanin: (—) excitation energy at 406.7 nm, and (- - -) excitation energy at 501.7 nm.

stretch with other modes. The vibration spectra at both excitation energies are characterized by strong peaks at 310 and 340 cm^{-1}. In blue copper proteins, such as plastocyanin, azurin, etc., Cu−S vibrations are typically observed in the 350−500 cm^{-1} region.[56,57]

The intensity-weighted average energy of the peaks $<\nu_{\mathrm{Cu-S}}>$ (effective stretching frequency), where $<\nu_{\mathrm{Cu-S}}> = \Sigma_i(I_i\nu^2)/\Sigma_i(I_i\nu_i)$, is used as an indicator of the Cu−thiolate bond strength.[56] The value of $<\nu_{\mathrm{Cu-S}}>$ for the red copper protein is 321 cm^{-1}. In comparison, the value of $<\nu_{\mathrm{Cu-S}}>$ for plastocyanin (a blue site) is 403 cm^{-1},[56] and for nitrite reductase (a green site), it is 383 cm^{-1}.[58] The above values indicate that the Cu−S(Cys) bond is weaker in red copper relative to the bond in blue and green copper sites. The decrease in the strength of the Cu−S(Cys) interaction from the Raman data is in agreement with the observed reduced covalency in S K-edge XAS data for nitrosocyanin relative to plastocyanin (section 3.3).

3.3. S K-Edge. The S K-edge XAS spectra of red copper and plastocyanin (as a reference) are shown in Figure 5. The spectra show a well-defined pre-edge feature at ∼2469 eV. This feature, present only in the spectrum of compounds which have a covalent interaction between S and a metal ion with a partially occupied metal d-manifold, is the 1s → ψ* (HOMO) transition.[10,59]

$$\psi^* \text{(HOMO)} = [1 - \alpha^2 - \beta^2]^{1/2}\ |\text{Cu 3d}> - \alpha\ |\text{S 3p}> - \beta\ |\text{other L}>$$

Due to the localized nature of the S 1s orbital and the fact that an s → p transition is electric-dipole allowed, this transition will gain intensity if the ψ* (HOMO) has a significant contribution from the S 3p orbital. This provides a direct probe of S 3p character (α^2) in the ψ* (HOMO) due to covalent overlap. Figure 5 shows both the normalized and renormalized

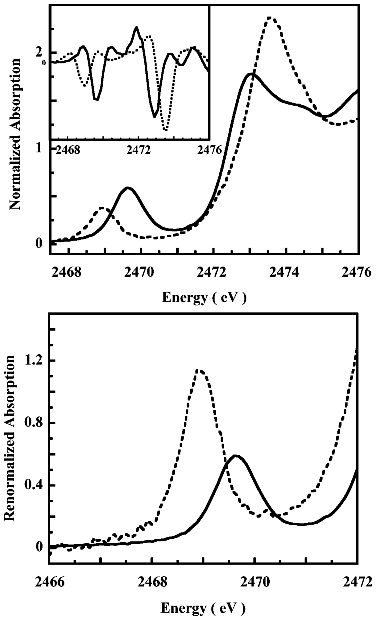

Figure 5. (A) Normalized S K-edge spectrum of red copper (—) compared with that of plastocyanin (- - -). Inset: Second derivative spectrum showing the shift in pre-edge position of 0.7 eV on going from plastocyanin to red copper. (B) Expanded section of the pre-edge region with the renormalized plastocyanin spectrum accounting for the presence of its total of three sulfurs.

S K-edge spectra. Renormalization is necessary to account for the presence of three sulfur atoms in plastocyanin versus one in red copper. Quantitation of the renormalized S K-edge pre-edge feature gives 20% sulfur character in the HOMO in red copper in comparison to 38% in plastocyanin. This difference is also supported by density functional calculations (section 4) and reflects a significantly weaker bonding interaction of the S(Cys) 3p orbital with the Cu 3d singly occupied orbital in red copper. This is in agreement with resonance Raman data and the elongation of the Cu−S(thiolate) bond distance from 2.1 Å in plastocyanin to 2.3 Å in red copper, as observed from crystallography and EXAFS (section 3.5).

The pre-edge transitions for plastocyanin and red copper occur at 2469.0 and 2469.7 eV, respectively (Figure 5). The pre-edge transition energy is affected by the relative energies of the S 1s orbital and the HOMO. The S 1s orbital is affected by changes in Z_{eff} felt by the sulfur nucleus, while the metal-based HOMO is affected by both Z_{eff} on the metal and changes in the Cu ligand field. The transitions resulting in the rising edge and edge structure are only influenced by the thiolate sulfur 1s orbital energy. The positions of the 1s → 4p transition in plastocyanin and red copper are at ∼2473.5 and ∼2473.0 eV, respectively. This transition has contribution from two methionines, and one cysteine, in plastocyanin,[9] and one cysteine in red copper. A comparison of the S K-edge XAS spectrum for noncoordinated methionine and cysteine (not shown)[60] estimates that the 1s → 4p transition would remain at the same energy (within resolution) due to the presence of two methionines in plastocyanin. This suggests that on going from red copper to plastocyanin, the S 1s core orbital has shifted ∼0.5 eV to a deeper binding energy (consistent with the increased S covalency). Combined with the pre-edge shift, this estimates a total shift of ∼1.2 eV to higher energy of the HOMO in red copper. This shift can be

---

(56) Blair, D. F.; Campbell, G. W.; Schnoover, J. R.; Chan, S. I.; Gray, H. B.; Malmström, B. G.; Pecht, I.; Swanson, B. I.; Woodruff, W. H.; Cho, W. K. *J. Am. Chem. Soc.* **1985**, *107*, 5755−5766.

(57) Han, J.; Adman, E. T.; Beppu, T.; Codd, R.; Freeman, H. C.; Huq, L.; Loehr, T. M.; Sanders-Loehr, J. *Biochemistry* **1991**, *30*, 10904−10913.

(58) Han, J.; Loehr, T. M.; Lu, Y.; Valentine, J. S.; Averill, B. A.; Sanders-Loehr, J. *J. Am. Chem. Soc.* **1993**, *115*, 4256−4263.

(59) DeBeer George, S.; Metz, M.; Szilagyi, R. K.; Wang, H. X.; Cramer, S. P.; Lu, Y.; Tolman, W. B.; Hedman, B.; Hodgson, K. O.; Solomon, E. I. *J. Am. Chem. Soc.* **2001**, *123*, 5757−5767.

(60) Frank, P.; Hedman, B.; Hodgson, K. O. Unpublished results.

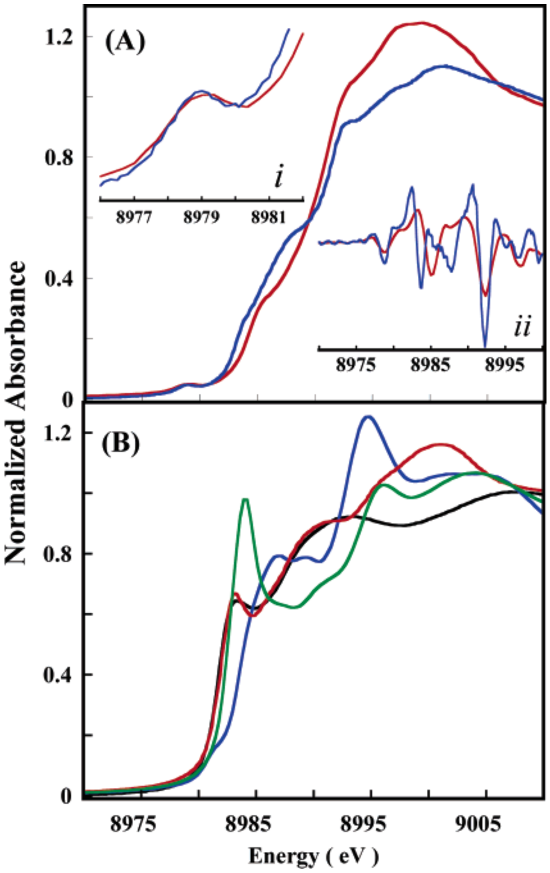

Figure 6. (A) Normalized Cu K-edge XAS spectrum of oxidized red copper (red line) compared to plastocyanin (blue line) (reference spectrum[10]). Inset *i* shows the pre-edge feature at 8979 eV, and *ii* shows the corresponding second derivative spectra. (B) Normalized Cu K-edge XAS spectrum of reduced red copper (red line) compared to two coordinate $[Cu(EDTB)_2]$-(ClO_2)[77] (green line), three-coordinate $[(C_6H_5)_4P]_2[Cu(SC_6H_5)_3]$[78] (black line), and four-coordinate $[Cu(2,5\text{-DTH})](ClO_4)$[79] (blue line) Cu(I) model complexes. The comparison clearly shows the three-coordinate nature of the reduced red copper site.

partially accounted for by the stronger ligand field felt by red copper compared to that of plastocyanin, which is estimated to be ~0.4 eV from the shift in the average energy of d → d bands in section 2.1. The rest (~0.8 eV) reflects the increase in coordination number from four in plastocyanin to five in red copper, which includes a short anionic carboxylate donor ligand. The increase in coordination number decreases the effective nuclear charge, putting the $d_{x^2-y^2}$ orbital at higher energy. Previous S K-edge studies show that an increase in coordination leads to an increase in the HOMO energy by ~0.6−1.0 eV.[61]

3.4. Cu K-Edge. Figure 6A shows a comparison of the Cu K-edge spectra of oxidized red copper and plastocyanin.[10] The energy of the weak pre-edge feature at ~8979 eV (expanded inset) is influenced by two factors, the Z_{eff} on the metal center and its ligand field. MCD studies show that the ligand field in red copper is ~0.4 eV higher than that in plastocyanin. The pre-edge of red copper, however, is only ~0.1 eV higher in energy as compared to that of plastocyanin. The remaining ~0.3 eV thus reflects Z_{eff}, which is lower in red copper due to the presence of additional donor ligands (H_2O and anionic O(Glu)). This is supported by the shift in the 1s → 4p transition (~8992 eV) to ~0.3 eV lower energy in red copper.

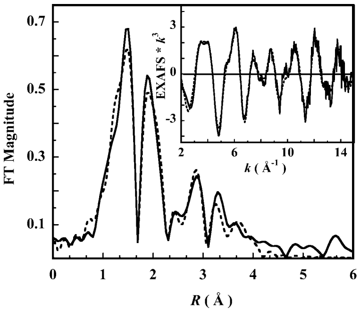

Figure 7. Fourier transforms (nonphase shift corrected) and EXAFS data (inset) of oxidized red copper protein. Data and fit represented by solid and dashed lines, respectively.

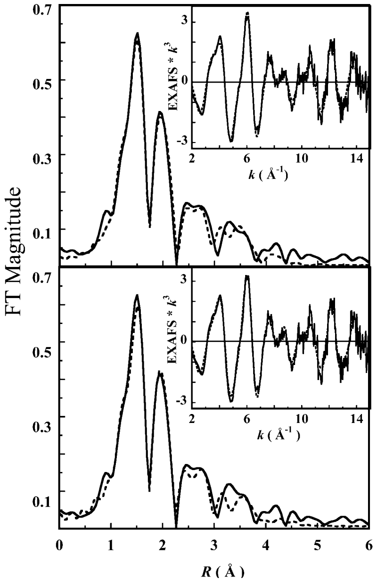

Figure 8. Fourier transform (nonphase shift corrected) and EXAFS data (inset) of reduced red copper protein. Data and fit represented by solid and dashed lines, respectively. Fit 1 (top) and fit 2 (bottom) represent two models differing in the representation of the weak ligand as histidine and glutamate, respectively.

Cu(I) compounds exhibit a characteristic edge structure with an intense pre-edge feature corresponding to the 1s → 4p transition at ~8984(±1) eV.[62] The energy position and intensity of this feature can be correlated to the ligation and site geometry around the cuprous ion.[62] A comparison of the edge structure of reduced red copper with previously reported spectra of representative two-, three-, and four-coordinate Cu(I) model complexes is shown in Figure 6B. The 1s → 4p feature appears at ~8983.3 eV and has an amplitude of 0.62. This shows that the edge structure of reduced red copper is consistent with three-coordinate geometry. This is supported by crystallography[16] and EXAFS (section 3.5), which show that the first coordination sphere in the reduced red copper site is effectively three-coordinate with an additional long 2.4 Å Cu−N/O interaction.

3.5. EXAFS. The EXAFS data for both the oxidized and reduced forms of red copper were Fourier transformed over $k = 2-15$ Å^{-1}. The EXAFS spectra and their Fourier transforms, with their corresponding fits, are given in Figures 7 and 8, and the oxidized and reduced EXAFS fit summaries are presented in Table 2. Fits were performed to the oxidized site spectrum using the 1.65 Å crystal structure as the initial model. The first

---

[61] DeBeer George, S. Ph.D. Thesis, Stanford University, 2001.

[62] Kau, L. S.; Spira-Solomon, D. J.; Penner-Hahn, J. E.; Hodgson, K. O.; Solomon, E. I. *J. Am. Chem. Soc.* **1987**, *109*, 6433−6442.

Table 2. EXAFS Curve Fitting Results for Oxidized and Reduced Red Copper Site

Oxidized Red Copper (first shell fit parameters)

coordination/path	R (Å)[a]	σ^2 (Å^2)[b]	E_0 (eV)	F[c]
3 Cu−N/O	1.96	58	−11.9	0.28
1 Cu−S	2.30	32		

Reduced Red Copper (first shell fit parameters)

Fit #	coordination/path	R (Å)[a]	σ^2 (Å^2)[b]	E_0 (eV)	F[c]
1	2 Cu−N/O	1.96	38	−11.90	0.28
	1 Cu−S	2.28	59		
	1 Cu−N	2.44	49		
2	2 Cu−N/O	1.96	40	−11.46	0.29
	1 Cu−S	2.28	46		

[a] Estimated standard deviations for the distances are about ±0.02 Å. [b] σ^2 values are multiplied by 10^5. [c] Error is given by $\sum[(\chi_{\text{obsd}} - \chi_{\text{calcd}})^2 k^6]/\sum[(\chi_{\text{obsd}})^2 k^6]$.

shell was fit by two Cu−N contributions and one Cu−O contribution at 1.96 Å. The addition of a Cu−S single scattering contribution at 2.3 Å modulated the first shell strongly and significantly improved the goodness of the fit. Multiple scattering paths from the imidazole rings were used to model the outer-shell components to the Fourier transform. The best fit was achieved by including both single and multiple scattering contributions from the outer shell of the two ligating imidazole rings. Inclusion of contributions from the long Cu−O(H_2O) bond at 2.25 Å observed in the crystal structure was not required by the data, as judged from successive fit comparisons. The pre-edge position (corrected for the shift in the edge positions), however, is shifted to higher energy in red copper compared to plastocyanin (section 3.4), consistent with a stronger ligand field in red copper, which supports the presence of this additional ligand. The S K-edge energy shift also reflects the increased coordination number of the red copper site.

Initial phase and amplitude parameters to fit the EXAFS data obtained from the reduced protein were generated from the crystallographic coordinates of reduced red copper protein at 2.3 Å. Least-squares refinements performed with these parameters allow for two distinct models with equally good fit results. In both approaches, the first shell was best modeled with two Cu−N/O contributions at 1.95 Å and one Cu−S contribution at 2.28 Å. Fit 1 further required Cu−N−C multiple scattering paths at 4.16 Å (see Supporting Information for complete EXAFS fit parameters). In addition, a contribution from a long-distance Cu−N/O interaction (at 2.45 Å) was required, and the corresponding multiple scattering from the histidine backbone was modeled at 4.72 Å. The outer shell from the imidazole rings contributed strongly to the fit and significantly improved the goodness of the fit. Fit 1 correlates with the crystal structure in that one of the histidine rings has moved away from the Cu center upon reduction (Figure 1C). Fit 2 does not include a long-distance Cu−N/O interaction, and the outer-shell Fourier transform intensity is modeled by multiple scattering interactions at 4.27 Å (Supporting Information). This fit supports a model where the coordinating histidine rings are at the same distance from the Cu(I) center and the glutamate has moved out of the coordination sphere. Fit 2 is consistent with the geometry-optimized structure obtained from DFT calculations (section 4.1.1). In both fits, however, inclusion of a H_2O is not required and one of the coordinating ligands has moved out to form a weak Cu−N/O interaction, which is consistent with the Cu K-edge data and the preference of Cu(I) for lower coordination number.

Table 3. Bond Distances and Angle at the Red Copper Site Obtained from Geometry-Optimized Structures, Crystal Structure (PDB files 1IBY and 1IBZ), and EXAFS

	Oxidized			Reduced		
	Opt.	X-tal	EXAFS	Opt.	X-tal	EXAFS
	Bond Length (Å)					
Cu−S(Cys95)	2.28	2.26	2.30	2.28	2.26	2.28
Cu−N(His103)	2.04	1.97	1.96	2.12	2.01	1.96
Cu−N(His98)	2.00	2.02	1.96	2.06	2.36	1.96
Cu−O(Glu60)	2.09	2.09	1.96	2.35	2.03	
Cu−H_2O	2.24	2.25				
	Dihedral Angle (deg)					
O(Glu)-Cu−S(Cys)−C_β	83.00	110.00		89	123	

4. Analysis

4.1. Density Functional Calculations. The experimental spectral features observed for the red copper center relative to those of the blue and green copper centers include the following: the ligand field transitions and the S(Cys) π- and pseudo-σ-to-Cu charge-transfer transitions are at higher energies, the pseudo σ is the most intense charge-transfer feature (the S(Cys) π charge transfer is most intense for blue copper), and the Cu−S(Cys) bond in red copper is longer, weaker, and less covalent. These data can now be used to evaluate electronic structure calculations and to obtain further insight into bonding. First, the oxidized and reduced red copper site structures are geometry optimized (section 4.1.1). Next, in the oxidized red copper site, the valence molecular orbital compositions are analyzed (section 4.1.2), and the transition energies and polarizations evaluated and correlated to experimental data (section 4.1.3). This provides spectral assignments associated with the unique spectroscopic and electronic structure of the oxidized red copper site. The ground- and excited-state electronic structures of the oxidized red copper site are then compared to those of the classical blue site of plastocyanin (section 4.2). The geometric and electronic structure contribution by water coordination in the red copper active site is evaluated (section 4.3). Finally, the geometry-optimized oxidized and reduced red copper active site structures are used in evaluating the reorganization energy associated with redox (section 4.4).

4.1.1. Geometry Optimization. Table 3 presents key bond distance and angle parameters for the oxidized and reduced red copper active site structures obtained from geometry optimizations (see section 2.5), X-ray crystallography (Figure 1A,C), and EXAFS. The geometry-optimized red copper site in the oxidized state (Figure 9A,i) is characterized by a Cu−S(Cys) bond at 2.28 Å, two Cu−N(His) bonds with typical Cu−N bond distance (∼2.00 Å), a water at 2.24 Å in the equatorial plane, and a Cu−O(Glu) bond at 2.09 Å in the axial position. The Cu−S bond in the red copper site is ∼0.14 Å longer than that in the geometry-optimized blue copper site (Figure S1, Supporting Information), indicating it is a weaker bond, which is consistent with EXAFS and S K-edge results and is supported by its lower effective stretching frequency in the resonance Raman data (section 3.2). The water molecule is in the trans position to the cysteine and comes off in the reduced site. Additionally, in going from the geometry-optimized oxidized (Figure 9A,i) to the reduced site (Figure 9A,ii), the axial Cu−O(Glu) bond gets longer (by 0.26 Å), while the S(Cys) and N(His) bond distances remain unchanged (in agreement with the EXAFS data; see Table 3). There is reasonable agreement

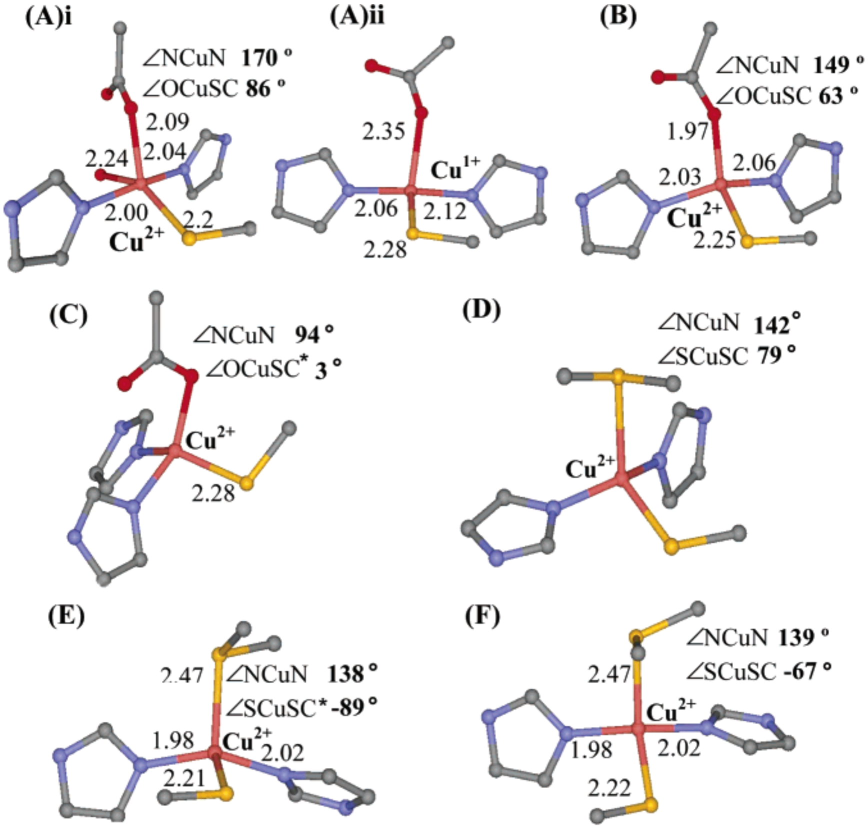

Figure 9. B(38HF)P86 optimized structures of computational models of (A,i) the oxidized five-coordinate red copper site, (A,ii) the reduced four-coordinate red copper site, (B) the oxidized four-coordinate (eliminating the water) red copper site, (C) the oxidized four-coordinate red site with dihedral angle ∠OCuSC constrained at 3°, (D) the oxidized four-coordinate red copper site with axial Glu substituted with Met, (E) the oxidized blue site with ∠SCuSC constrained at −89°, and (F) the oxidized blue site with ∠NCuN increased to 139°.

between DFT-calculated and experimentally observed structures, implying that the computational structure is a good model of the red copper site in nitrosocyanin.[63a]

First shell distances are [Cu−S(Cys) 2.25 Å, Cu−N(His) 2.04 Å, Cu−N(His) 2.05 Å, Cu−O(Glu) 1.98 Å] compared to the distances in Table 3, column 1. The somewhat shorter Cu−O(Glu) distance reflects the lack of the H_2O (fifth) ligand in the optimization.

4.1.2. Ground-State Wave Function. The ground-state bonding description of the oxidized red copper active site is presented in Figure 10A. The spectroscopically adjusted DFT calculations using the BP(38HF)86 functional give a ground-state description which is in good agreement with the experimentally derived ground-state properties. The nature of bonding between the Cu and the S(Cys) is σ, with a S 3p covalency of ∼20%, consistent with S K-edge XAS data. The σ ground state of the red copper site is in agreement with the observed absorption spectra in that the σ charge transfer is most intense (Figure 2). The total contribution from the two N(His) is 9%, and the O(Glu) and water are 1% and 3%, respectively. The equatorial S(Cys), the two N(His), and water are ligated along the four lobes of the Cu $3d_{x^2-y^2}$ orbital. A detailed comparison of the ground-state wave function and properties of the red and blue copper site is presented in section 4.3.

In the modified crystallography-based (and subsequently geometry optimized) computational model where the water is replaced by a hydroxide, the S(Cys) covalency in the ground-state wave function is 8%, less than half the experimental S(Cys) covalency. The red copper site is thus well modeled with water being the fifth ligand, consistent with the absence of any pH dependence (vide supra). The high-resolution (1.65 Å) crystal structure suggests that the ligated water at the red copper active

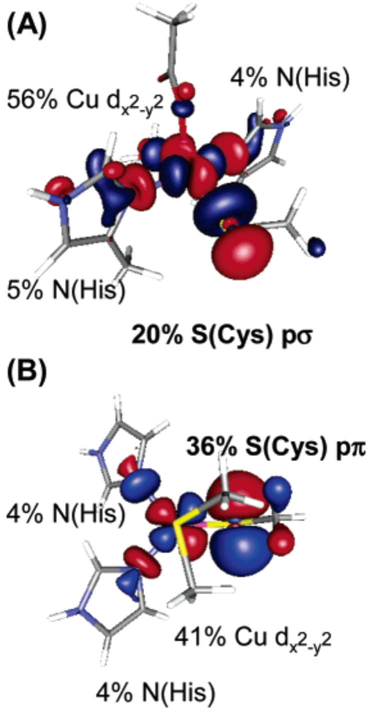

Figure 10. Contour plots for ground-state wave function of the red copper site in nitrosocyanin (A) and the blue copper site in plastocyanin (B).

Table 4. Results of ADF Calculations for the Highest Valence Orbitals at the Red Copper Site

		Orbital Contribution											
MO labels	energy (eV)	$d_{x^2-y^2}$	d_{xz}	d_{yz}	d_{z^2}	d_{xy}	Spsσ	Sπ	N(His)	H_2O	O(Glu)	ΔSCF (cm^{-1})	Pol.
$d_{x^2-y^2}$	−0.09	56	0	0	1	0	16	0	9.3	2.7	0.75		
d_{xz}	−0.98	0	49	0	8	0	0	27	0.1	1.6	5.2	7800	*z*
d_{yz}	−2.17	0	1	83	4	0	0	4.5	1.5	0.2	1.2	*a*	*y*
d_{z^2}	−1.52	0	5	2	69	0	5	5	0.5	1	0.9	12700	*x*
d_{xy}	−2.62	5	0	0	0	77	2.4	2	1	0.2	0.3	15500	*x*
Cys π	−2.35	0	29	4	0	0	0	50	0.3	1.3	3.7	24500	
Cys σ	−3.05	13	0	0	5	8	53	0	0.2	2.5	1.9	28500	

[a] The d_{yz} excited state converged to other states. See ref 63.

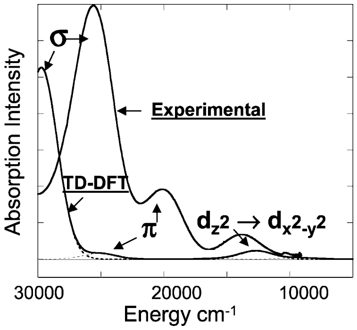

Figure 11. Calculated (TD-DFT) and experimental electronic absorption spectra of red copper.

site is stabilized due to a hydrogen bond to the uncoordinated oxygen of the axial glutamate (Glu60).

4.1.3. Excited States. Table 4 summarizes the wave function characters and ΔSCF transition energies for the highest valence orbitals of the oxidized red copper site. The calculations predict the charge-transfer transitions at energies (24,500 and 28,500 cm^{-1}) higher than those of the ligand field transitions (lying in the 7000−15500 cm^{-1} range). Also, the S(Cys) pseudo $\sigma \rightarrow$ Cu $d_{x^2-y^2}$ charge-transfer transition is calculated to be at ~4000 cm^{-1} higher energy than that of the π charge-transfer transition, in reasonable agreement with experiment (~5000 cm^{-1}). The calculated ligand field splitting order is $d_{x^2-y^2} > d_{xz} > d_{z^2} > d_{yz} > d_{xy}$, where *x* and *y* are along Cu−S and Cu−N bonds, respectively, and *z* is along the axial Cu−O(Glu) bond. [63b]

Figure 11 compares the calculated (TD-DFT) and the experimental electronic absorption spectra of red copper and lists the principal electronic excitations which contribute to the electronic transitions. The TD-DFT calculations show a good correlation with the observed spectral pattern: the ligand field block at lowest energy, followed by the cysteine π, and at higher energy the more intense pseudo σ charge-transfer transition.

It is interesting to note the high intensity ($\epsilon \sim 7000$ M^{-1} cm^{-1}) of the pseudo σ charge transfer in the red copper site even though it is less covalent than a blue copper site where the π charge transfer is lower in intensity ($\epsilon \sim 5000$ M^{-1} cm^{-1}). The absorption intensity is a reflection of the ligand character in both the metal-based acceptor orbital and the ligand-based donor orbital. When going from the blue to red copper site, the S(Cys) character in the acceptor orbital has reduced (from the S K-edge XAS data, blue copper 38%, red copper 20%), while the S(Cys) character in the donor orbital (S(Cys) π in blue and pseudo σ in red) has increased (DFT results, 39% in blue, Table S1 Supporting Information, to 53% in red, Table 4). This increased S(Cys) 3p character in the pseudo σ donor orbital in red copper results in the high intensity of this transition even with the lowered HOMO covalency.

In the ligand field region of red copper, band 3 is most intense in the absorption spectrum in Figure 2. This band is assigned to the $d_{z^2} \rightarrow d_{x^2-y^2}$ transition, as only the d_{z^2} orbital has significant S(Cys) pseudo σ character (5%, see Table 4). TD-DFT calculations also indicate that the most intense ligand field transition is the $d_{z^2} \rightarrow d_{x^2-y^2}$ transition (Figure 11). This mixing provides transition intensity polarized along the Cu−S bond (*x*-axis). Band 3 is of opposite sign to bands 1 and 2 in the MCD spectrum (Figure 2). States that are close in energy, with perpendicular transition moments, and are spin−orbit coupled to form a derivative-shaped pseudo-A MCD signal that is composed of *C*-term transitions with opposite signs. The transition densities, obtained from the product of the donor and acceptor molecular orbitals (Figure S2, Supporting Information), give the direction of the dipole moment for each transition (listed in Table 4). The *x*-polarized (along the Cu−S(Cys) bond) $d_{z^2} \rightarrow d_{x^2-y^2}$ transition can spin−orbit couple to the *z*-polarized (along the O(Glu)−Cu bond) $d_{xz} \rightarrow d_{x^2-y^2}$ transition ($\hat{L}_y d_{z^2} = i\sqrt{3}d_{xz}$) and the *y*-polarized (along the Cu−N(His) bonds) $d_{yz} \rightarrow d_{x^2-y^2}$ transition ($\hat{L}_x d_{z^2} = -i\sqrt{3}d_{yz}$). The d_{xz} orbital will be the SOMO-1 as it is destabilized by a π interaction with the S 3p orbital (Figure S3A, Supporting Information). Band 1 is thus assigned as the $d_{xz} \rightarrow d_{x^2-y^2}$ transition, and the next higher energy band 2 is assigned as the $d_{yz} \rightarrow d_{x^2-y^2}$ transition. The $d_{xy} \rightarrow d_{x^2-y^2}$ transition has the same polarization as the $d_{z^2} \rightarrow d_{x^2-y^2}$ transition and can also spin−orbit couple to d_{xz} and d_{yz}. Band 4, which has the same MCD sign as band 3, is assigned as the $d_{xy} \rightarrow d_{x^2-y^2}$ transition. The experimentally observed order of the ligand field transitions are reasonably reproduced[63] by the density functional calculations (ΔSCF, Table 4).

4.2. Electronic Structure Correlation of Oxidized Red and Blue Cu Sites. 4.2.1. Ground State. The ground-state wave function of the red copper site (Figure 10A) exhibits some dramatic differences relative to that of the blue copper site (Figure 10B). The primary difference is the nature and strength of the Cu−S(Cys) interaction. The red copper site is characterized by a σ−copper thiolate interaction and relatively less covalent (20% S 3p) Cu−S(Cys) bond, while the blue copper

---

(63) (a) Geometry optimization performed on an oxidized model using the EXAFS-derived distances converges to a structure which is in reasonable agreement with the optimized structure obtained from the crystal structure model. (b) The ΔSCF calculations did not converge for the d_{yz} excited state. The Slater transition-state energies (removal of 0.5 electron from a given orbital and reconverging) predict the d_{yz} transition energy at 15,977 cm^{-1}. The other transition energies obtained by the Slater transition-state method are within ~150 cm^{-1} of the ΔSCF energies. However, the predicted d_{yz} transition energy is higher than the experimentally observed energy. This is due to the longer Cu−N(His) bonds in the geometry-optimized structure compared to the EXAFS structure (see Table 3), which results in less (by ~2000 cm^{-1}) destabilization of the d_{yz} orbital, leading to its higher transition energy. The corrected d_{yz} transition energy is at 13,900 cm^{-1}.

site has a S(Cys)−Cu π bond which is very covalent (38% S 3p). There is also a sizable increase of 6850 cm^{-1} in the pseudo σ charge-transfer energy (from 18 700 cm^{-1} in plastocyanin to 25,550 cm^{-1} in nitrosocyanin) and an increase of 3650 cm^{-1} for the π charge-transfer energy (16,700 cm^{-1} in plastocyanin versus 20,350 cm^{-1} in nitrosocyanin). Charge-transfer transitions generally increase by ~5000 cm^{-1} with an increase in coordination number due to the decrease in Z_{eff} at the metal center. Also, the S(Cys) $\pi-\sigma$ splitting increases in red copper (from 2000 cm^{-1} in plastocyanin to 5200 cm^{-1} in nitrosocyanin), as the blue copper site has a strong π and weak σ Cu−S(Cys) interaction, while for the red copper site, this is reversed, weakening the π band and stabilizing the energy of the σ bonding orbitals.

From S K-edge XAS and resonance Raman data, the Cu−S(Cys) bond in the red copper site is weaker than that in the blue copper site. The variation in the stretching force constant with bond length can be described using Badger's[64] rule:

$$k = 1.86(r_{\mathrm{e}} - d_{\mathrm{ij}})^{-3}$$

where r_{e} is the equilibrium bond length, and constant d_{ij} is fixed for bonds between atoms from row i and j of the periodic table. Using the Cu−S bond distance for the two sites (2.26 Å for nitrosocyanin and 2.07 Å for plastocyanin), the stretching frequency in red copper is estimated based on that of the blue copper site (403 cm^{-1}). The calculated value of 245 cm^{-1} is lower than the experimental value of 321 cm^{-1}, suggesting that the σ overlap (versus π overlap in blue copper) of the S p orbital with Cu $d_{x^2-y^2}$ in red copper contributes to the observed bond strength.

Relative to the blue copper site, the red copper site has additional donor contributions from the anionic glutamate and the water ligands. These would also lead to reduced net donation of the thiolate ligand to the Cu and weaken the Cu−S bond. The difference in the red relative to the blue copper site clearly reflects the presence of the fifth ligand (H_2O), which greatly influences the electronic structure.

4.2.2. Ligand Field. Figure 12 presents the valence molecular levels of nitrosocyanin and plastocyanin derived from spectroscopy.[65] This comparison demonstrates that the entire d-manifold is higher in energy in the red copper site relative to the blue site. Figure 12 shows that the highest singly occupied molecular orbital ($d_{x^2-y^2}$) in blue copper is greatly stabilized in going to the red site (note the coordinate axis change; in the blue copper site, the Cu−S bond bisects the x and y axes, while in red copper, Cu−S and Cu−N bonds are along x and y, respectively). The strong S(Cys) pπ−Cu $d_{x^2-y^2}$ interaction in the blue copper site is lost in the red copper site resulting in this dramatic change. In contrast, the d_{xy} orbital of blue copper is destabilized due to substantial σ interaction with the S(Cys) 3p orbital (Figure 10), making this the highest singly occupied redox active orbital in red copper. This interchange of the d orbitals results from a key geometric difference between the red and blue copper sites.

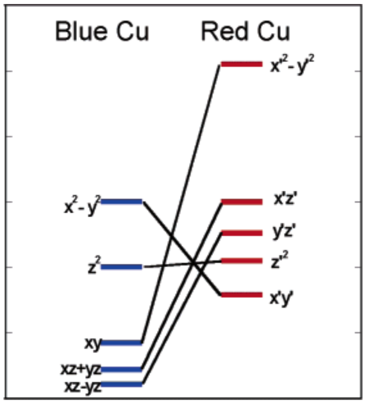

Figure 12. Valence molecular levels of red and blue copper sites. Experimental ligand field transition energies used for ordering. The energy level diagram of the blue and red copper sites has been aligned to a C−H (on imidazole ring) level obtained from density functional calculations. In this comparative scheme, the red copper site levels are marked primed (′) as the coordinate system for the red copper site is rotated (45°) relative to the blue copper site coordinate system. (The primes have been dropped elsewhere in the text when only the levels of the red copper site have been referred to.)

Scheme 1. Equatorial (NNS) Plane of the Blue (left, the S is eclipsed by the C) and Red (right) Copper Sites[a]

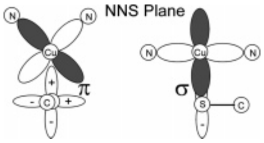

[a] S(Cys)−C bond ⊥ to NNS plane in blue and in the NNS plane in red copper. The blue copper site has two S p orbitals, while the red copper site has one S p orbital in this plane available to interact with copper.

As seen in Figure 1, in blue copper, the S(Cys)−C$_\beta$ bond is parallel to the axial Cu−S(Met) bond, perpendicular to the equatorial Cu−S(Cys)−N(His)−N(His) plane. This orients the two S 3p orbitals ⊥ to the S−C bond in the equatorial plane and thus interacting with the $d_{x^2-y^2}$ orbital (Scheme 1, left). In contrast, in the red copper site, the S(Cys)−C$_\beta$ bond is in the equatorial plane. As a result, only one of the S 3p orbitals is in the equatorial plane and available for bonding with a Cu d orbital in the plane, forming the Cu−S(Cys) pseudo σ bond. The d_{xz} orbital is additionally destabilized in the red relative to blue copper site because of its π interaction with the second (out of plane) S 3p orbital (see Supporting Information, Figure S3A,B).[66] Thus, the orientation of the cysteine ligand relative to the equatorial plane is key in modulating the electronic structure of the red relative to blue copper sites.

The changes observed in the ligand field region can be correlated to the EPR parameters. The g value expressions for a singly occupied Cu 3$d_{x^2-y^2}$ HOMO from ligand field theory[67] are directly proportional to the amount of metal d-character in the x^2-y^2 and xy orbitals (for g_z) and inversely to the ligand field transition energies. The experimental energy of the $d_{xy} \rightarrow d_{x^2-y^2}$ transition is higher (by 4200 cm^{-1}) in the red relative to that in the blue copper site. However, the g_z value for the red and the blue copper sites are very similar (2.24 and 2.23, respectively), indicating an increased Cu character in the HOMO

---

(64) Badger, R. M. *J. Chem. Phys.* **1934**, *2*, 128−131.

(65) The energy level diagram of the blue and red copper sites has been aligned to a C−H (on imidazole ring) level obtained from density functional calculations. In this comparative scheme, the red copper site levels are marked primed (′) as the coordinate system for the red site is rotated (45°) relative to the blue copper site coordinate system. (The primes are not included elsewhere in the paper when only the levels of the red copper site are considered.)

(66) Note that the d_{z^2} level undergoes little change in going from the blue to the red site. The destabilization due to increased coordination appears to be compensated by a bonding interaction with the d_{xz} orbital (which forms the π bond with the thiolate, Figure S3C, Supporting Information).

(67) McGarvey, B. R. In *Transition Metal Chemistry*; Carlin, R. L., Ed.; Marcel Dekker, New York, 1966; pp 89−201.

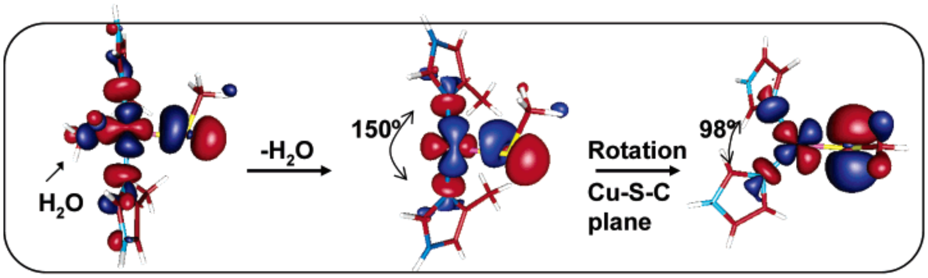

Figure 13. Contour plots for ground-state wave function of (A) five-coordinate red copper and (B) four-coordinate (water ligand eliminated) red copper and (C) blue copper. The axial ligands are not shown to visualize clearly the bonding differences in the red and blue copper sites.

of red copper. This is a reflection of reduced S(Cys) covalency and is consistent with S K-edge data (from 40% in blue to 20% in red copper).

Relative to that in plastocyanin, the A_z value is higher in nitrosocyanin ($|140| \times 10^{-4}$ cm^{-1} versus $|63| \times 10^{-4}$ cm^{-1} in plastocyanin). The hyperfine coupling constant depends on three factors: (a) Fermi contact, which is due to the unpaired spin density at the Cu nucleus; (b) direct spin dipolar coupling, which arises from the interaction of the electron spin with the nuclear spin of the metal; and (c) indirect (orbital) dipolar coupling, which is due to coupling of the electron orbital magnetic moment and the nuclear spin of the metal and is related to the deviation of the g values (Δg) from 2.0023.[67]

$$A_{\|} = P_{\mathrm{d}}((-\kappa - 4/7)\alpha^2 + 3/7\Delta g_{\perp} + \Delta g_{\|})$$

$$A_{\perp} = P_{\mathrm{d}}((-\kappa + 2/7)\alpha^2 + 11/14\Delta g_{\perp})$$

where P_{d} is 396×10^{-4} cm^{-1}; κ is the Fermi contact term, and α^2 is the percent metal character in the $d_{x^2-y^2}$ derived molecular orbital. Using experimental g values, the increase in hyperfine coupling corresponds to an increase of the metal character from 41 to 56%, consistent with reduced S(Cys) covalency (in S K-edge data, from 40% in blue to 20% in red copper).

4.3. Water Coordination at the Red Copper Site. Key structural differences between red and blue copper sites are the additional water coordination at the red copper site, the axial ligand in red is O(Glu) versus S(Met) in blue, the N(His)−Cu−N(His) angle is 156° in red (Figure 1A) versus 99° in blue (Figure 1B), and the O(Glu)−Cu−S(Cys)−C$_\beta$ dihedral angle is 110° in red relative to a 3° S(Met)−Cu−S(Cys)−C$_\beta$ dihedral angle in blue. The larger N−Cu−N angle will be referred to here as the open configuration, and the larger O(Glu)−Cu−S−C$_\beta$ dihedral angle (S−Cu−S−C$_\beta$ in blue copper) as the down orientation. Associated with these geometric differences, the nature of the ground state is also dramatically different, σ in the red copper and π in the blue copper (Figure 10). To determine the protein contributions to these changes in the geometric and electronic structure between red and blue copper sites (red = σ ground state, down orientation, open configuration; blue = π ground state, up orientation, closed configuration), electronic structure calculations have been performed on a series of computational models of red and blue copper, systematically evaluating the different structural perturbations.

To evaluate the effects of the coordinated water on the geometric and electronic structure of the red copper site, the water was eliminated and the site geometry was reoptimized. This four-coordinate (oxidized red copper minus the water, Figure 9B) site is characterized by a Cu−S bond at 2.25 Å, the Cu−N bonds at 2.03 and 2.06 Å in the equatorial plane, and a Cu−O bond at 1.97 Å in the axial position. The N−Cu−N angle is 149°, and the O−Cu−S−C dihedral angle is 63°, that is, an open configuration and down orientation similar to the five-coordinate red copper site with the water (in the five-coordinate geometry-optimized structure, the N−Cu−N angle is 170° and the O−Cu−S−C dihedral angle is 86°; Figure 9A,i). The four-coordinate red site still has the S−Cu σ bonding interaction (Figure 13, middle). Thus, eliminating the water does not greatly change the geometric and electronic structure relative to the five-coordinate site. Whereas in the four-coordinate red copper site, on constraining the dihedral angle O−Cu−S−C angle at the corresponding blue copper value (i.e., the up orientation), and on geometry optimization with this fixed dihedral angle, the N−Cu−N bond angle decreases to 94° (Figure 9C), similar to that for the closed blue copper configuration (Figure 1B). This change indicates that with the S−C bond perpendicular to the equatorial plane, the N−Cu−N angle decreases (from 149 to 94°, Figure 9C), which would favor the π interaction between the S p and Cu d orbitals in the equatorial plane. Finally, on substituting the axial glutamate to a methionine in the four-coordinate red site (red copper site minus the water), the optimized structure still has the open 142° configuration and down 79° orientation (Figure 9D), suggesting that the axial ligand is not the critical factor in determining the electronic structure.

NOTE: To evaluate the effect of the difference in the orientation of the histidine imidazole rings in red copper relative to that in blue copper, the following have been considered. (1) The orientations of the imidazole rings in red copper were changed to that of the blue copper site, and when the structure was reoptimized, the imidazole rings assumed a perpendicular orientation to the NNS plane similar to that of the optimized red copper structure. (2) The four-coordinate (water eliminated) red copper site optimizes with the imidazole rings perpendicular to the NNS plane (Figure 9B). (3) When the direction of the S(Cys)−C bond is constrained to be perpendicular to the NNS plane, the structure optimizes with the imidazole rings oriented similar to the blue copper site (Figure 9C). These indicate that the orientation of the S(Cys)−C bond relative to the NNS plane affects the orientation of the imidazole rings due to steric interactions.

The optimized structure of the blue copper active site has an equatorial N−Cu−N angle of 100° and a S−Cu−S−C dihedral angle of 0.5° (Figure S1, Supporting Information). To mimic the red copper active site, first, the S−Cu−S−C dihedral angle is increased to a down orientation and the structure geometry optimized with this dihedral angle constraint. Interestingly, the

N−Cu−N angle opens to 138° (Figure 9E), similar to the four-coordinate red copper site (Figure 9B), again indicating that with the S−C bond in the equatorial plane, the favored orientation is open, and this corresponds to a bonding scheme that involves a σ interaction between the Cu d and the S p orbital (Figure S4, Supporting Information). Second, when the N−Cu−N angle of the blue copper site is increased (i.e., open configuration) and subsequently geometry optimized without any constraints, the resulting optimized structure has a N−Cu−N angle of 139° and a S−Cu−S−C dihedral angle of −67° (Figure 9F), reflecting an open configuration and down orientation, as in the red copper site.

In the series of geometry optimized structures obtained above, the open configuration−down orientation σ structure and the closed configuration−up orientation π structures are close in energy (difference ~2 kcal/mol), indicating that they both represent comparably stable structures. The opened-up and the closed-down structures are less favored by 13 and 38 kcal/mol, respectively. The latter is more unfavorable as it loses the π interaction between the S p and the Cu $d_{x^2-y^2}$ orbitals. To bring these geometry optimization computational results into context, it is important to consider the protein sequences in the region of the active site in blue and red copper proteins that lead to the unique geometric and electronic structure at each site (see Discussion).

4.4. Contribution of the Water Ligand to Redox. Nitrosocyanin, being 65% homologous[17] to blue copper proteins, is a potential electron transfer protein. The geometric and electronic structure of the blue copper active site is tuned for fast, long-range electron transfer. However, the red copper site exhibits some marked differences in the geometric and electronic structure relative to that of the blue copper site, primarily due to the additional coordinated water molecule in the red copper active site. The contribution of the water ligand to the thermodynamic and kinetic properties of electron transfer is evaluated in this section.

According to the Marcus[68] theory, the rate of electron transfer is dependent on H_{DA}, the electronic coupling between the donor and acceptor, $\Delta G^{\ddagger}$, the thermodynamic driving force, that is, the difference in reduction potentials ($E°$) between electron donor and acceptor, and λ, the reorganization energy associated with the active site geometry change (λ_{inner}) and reorientation of solvent dipoles (λ_{outer}, where $\lambda = \lambda_{inner} + \lambda_{outer}$) with redox. The rate of electron transfer is enhanced by maximizing H_{DA} while minimizing the sum of ($\Delta G^{\ddagger} + \lambda$). The reduction potential of nitrosocyanin is 85 mV, which is ~200 mV lower than the range of most blue copper proteins. Several factors contribute to this lower potential. These include the differences in the protein environment, the anionic O(Glu) ligand (relative to the neutral S(Met) in blue copper), and the additional water ligand in the red copper site. $E°$ values of equivalent sites can vary over a range of 450 mV due to differences in the protein matrix.[7] The effect due to the anionic axial ligand in the same protein environment has been observed experimentally in mutant studies[69,70] of azurin ($E°$(wild-type azurin) = 290 mV, and $E°$-(Met121Glu) = 184 mV, where the axial S(Met) has been replaced by an anionic oxygen donor). The charge on the glutamate stabilizes the oxidized state and lowers the potential. PCM calculations on the blue and red copper redox couples (modeled with and without the water ligand) indicate that the contribution of the anionic O(Glu) is relatively stronger in lowering the reduction potential than the contribution of the additional water ligand in red copper.

Facile outer-sphere electron transfer requires large H_{DA} and low reorganization energy. This is observed for blue copper electron transfer proteins.[7] H_{DA} (proportional to the covalency, from S K-edge 40% in blue versus 20% in red) is reduced by half going from the blue to the red site and would lower the rate of electron transfer. The inner-sphere reorganization energy is determined by the structural changes in the first coordination sphere of the metal ion and can be predicted using density functional calculations and measured experimentally.[71,73,74] The reorganization energies of blue copper active sites have been estimated to be 0.6−0.8 eV, in contrast to the large λ_i (~1.4 eV) associated with normal copper complexes.[7,71−74] For the five-coordinate oxidized red copper active site, the reorganization energy upon reduction is calculated to be 2.2 eV. This appreciable increase in reorganization energy in the red copper site derives from the fact that the water, which is coordinated ($Cu-OH_2 = 2.15$ Å) in the oxidized state, is not bound ($Cu-OH_2 = 3.90$ Å) in the reduced state. If the red copper site is modeled as a four-coordinate site (i.e., without the water in both the oxidized and reduced site), the reorganization energy is calculated as 1.2 eV. Thus, the water ligation at the red copper active site leads to ~1 eV increase in the inner-sphere reorganization energy, making the red copper site unfavorable for fast outer-sphere electron transfer relative to a typical blue copper site.

5. Discussion

The electronic structure of the red copper site of nitrosocyanin, which contains an axial glutamate and an equatorial water ligation, has now been defined. The spectroscopic features of the red copper site are dramatically different compared to those of the typical blue copper site. In nitrosocyanin, the shift of the d → d transitions to ~3350 cm^{-1} higher energy than those of plastocyanin indicates that the site is more tetragonal due to the additional equatorial water ligation. The increased S(Cys) → Cu charge-transfer transition energies reflect the effect of increased coordination in red copper relative to the blue copper site. The fact that the S(Cys) pseudo $\sigma \rightarrow$ Cu charge-transfer transition (~390 nm) is 3-fold more intense than the S(Cys) $\pi \rightarrow$ Cu charge-transfer transition indicates that the ground state is characterized by a S(Cys)−Cu σ bond, in contrast to the π bond in blue copper sites. Further, compared to that in blue copper, the S(Cys)−Cu bond is longer and weaker in the red copper site. Also, the thiolate covalency of the red copper site is half that of the blue copper site. These characteristic features of nitrosocyanin are the manifestation of increased coordination associated with the additional water ligand at the red copper site.

---

(68) Marcus, R. A.; Sutin, N. *Biochim. Biophys. Acta* **1985**, *811*, 265−322.

(69) Andrew, C. R.; Yeom, H.; Valentine, J. S.; Karlsson, B. G.; Bonander, N.; van Pouderoyen, G.; Canters, G. W.; Loehr, T. M.; Sanders-Loehr, J. *J. Am. Chem. Soc.* **1994**, *116*, 11489−11498.

(70) Karlsson, B. G.; Tsai, L. C.; Nar, H.; Sanders-Loehr, J.; Bonander, N.; Langer, V.; Sjölin, L. *Biochemistry* **1997**, *36*, 4089−4095.

(71) Olsson, M. H. M.; Ryde, U.; Roos, B. O. *Protein Sci.* **1998**, *7*, 2659−2668.

(72) Ryde, U.; Olsson, M. H. M. *Int. J. Quantum Chem.* **2001**, *81*, 335−347.

(73) Winkler, J. R.; Wittungstafshede, P.; Leckner, J.; Malmström, B. G.; Gray, H. B. *Proc. Natl. Acad. Sci. U.S.A.* **1997**, *94*, 4246−4249.

(74) Crane, B. R.; Di Bilio, A. J.; Winkler, J. R.; Gray, H. B. *J. Am. Chem. Soc.* **2001**, *123*, 11623−11631.

The contributions of the water ligand to the redox properties of the red copper site have been evaluated. The significant contribution is to the inner-sphere reorganization energy, which increases by ∼1 eV relative to that in the typical blue copper site. An increase in reorganization energy is unfavorable for facile electron transfer. The coordinated water also contributes (along with the anionic glutamate ligand) to the relatively low reduction potential of the red copper site. The reduced red copper site loses the water and has an open coordination position, which could be a potential site for substrate or small molecule binding. Preliminary data[80] suggest that red copper protein is, in fact, slow with outer-sphere and rapid with inner-sphere electron-transfer reagents (the opposite behavior of blue copper proteins).

It is interesting to consider the analogy between nitrosocyanin and cytochrome *c*′. Cytochromes are generally six-coordinate heme sites, which are efficient in electron transfer. Unlike other cytochromes, cytochrome *c*′ has an open coordination position in the active site. Cytochrome *c*′ is believed to be an electron-transfer protein although the reaction partners have not been identified. Recent studies[82,83] have shown that cytochrome *c*′ binds small neutral molecules, such as NO, and functions as an NO carrier or an NO reductase. Red copper protein, a member of the electron-transfer cupredoxin family, also has an open coordination position (a water molecule is bound in the oxidized state and is eliminated in the reduced state), which could be a potential binding/reactivity site for small molecules. Recent physiological and proteomic experiments[75] have shown that when *Nitrosomonas europaea* is at low oxygen and high nitrite concentrations, there is evidence for increased NO production via denitrification. Interestingly, significantly higher concentrations of nitrosocyanin are expressed, suggesting that it could be involved in the denitrification process. The genome sequence[76] indicates the presence of a FNR protein recognition sequence (fumarate−nitrate reduction proteins are transcription regulators associated with the shift from aerobic to anaerobic growth in the bacteria) in the promoter region of nitrosocyanin, indicating that nitrosocyanin expression is increased under anaerobic conditions when nitrite acts as the terminal electron acceptor, again suggesting that nitrosocyanin could be involved in denitrification.

The comparison of the sequences of amino acids at the red (nitrosocyanin) and blue (plastocyanin) copper active sites shows that His98 and Cys95 are sequentially and structurally conserved (in blue, His87 and Cys84, respectively; see Figure 1A,B) between red and blue copper proteins, while equatorial His103 and axial Glu60 in the red copper site replace the axial Met92 and the equatorial His37, respectively, of the blue copper active site. Thus, on going from the blue site to the red site, these sequence changes result in the S(Cys)−C_β bond being oriented in the equatorial Cu−N(His)−N(His) plane in the red copper site (Figure 13), resulting in the larger O(Glu)−Cu−S(Cys)−C_β dihedral angle (down orientation).[81] From the above geometry optimizations, the down orientation of the S(Cys)−C_β bond leads to σ bonding of S(Cys) and Cu and opens the N(His)−Cu−N(His) bond angle (173° in red versus 100° in blue) to allow the histidines to overlap with the Cu $d_{x^2-y^2}$ orbital, creating an open coordination position for exogenous water binding. This provides a reasonable explanation for the coordination of the additional water ligand at this open position in the red copper site. Importantly, this clearly indicates the role of the protein in determining the geometric and electronic structure of the active site in red versus blue copper centers.

Acknowledgment. This research was supported by NSF Grant CHE-9980549 (E.I.S.), NIH Grant RR-01209 (K.O.H.), and NSF Grant 9723608 (A.B.H.). SSRL operations are funded by the U.S. Department of Energy, Office of Basic Energy Sciences. The Structural Molecular Biology program at SSRL is supported by the National Institutes of Health, National Center for Research Resources, Biomedical Technology Program, and Department of Energy, Office of Biological and Environmental Research.

Supporting Information Available: Complete EXAFS curve fitting results, tables of Cartesian coordinates for the density functional calculations, the B(38HF)P86 optimized structure of the computational model of the oxidized blue copper site and the reduced red copper site, orbital compositions for the valence orbitals obtained from ADF calculations at the blue copper center, the transition densities for the ligand field transitions, and the contour plots for the d_{z^2}, d_{xz} antibonding, and the Cu−S pπ bonding orbitals, and orbital contour plot for the ground-state wave function of the blue copper site constrained at 89°, showing the σ interaction between the Cu d and S p orbital. This material is available free of charge via the Internet at http://pubs.acs.org.

JA044412+

---

(75) Schmidt, I.; Steenbakkers, P. J. M.; op den Camp, H. J. M. *J. Bacteriol.* **2004**, *186*, 2781−2788.

(76) Chain, P.; Lamerdin, J.; Larimer, F.; Regala, W.; Lao, V.; Land, M.; Hauser, L.; Hooper, A. B.; Klotz, M.; Norton, J.; Sayavedra-Soto, L.; Arciero, D. M.; Hommes, N.; Whittaker, M. *J. Bacteriol.* **2003**, *185*, 2759−2773.

(77) Hendriks, H. M. J.; Birker, P. J. M. W. L.; Van Rijn, J.; Verschoor, G. C.; Reedijk, J. *J. Am. Chem. Soc.* **1982**, *104*, 3607−3617.

(78) Coucouvanis, D.; Murphy, C. N.; Kanodia, S. K. *Inorg. Chem.* **1980**, *19*, 2993−2998.

(79) Olmstead, M. M.; Musker, W. K.; Kessler, R. M. *Inorg. Chem.* **1981**, *20*, 151−157.

(80) Basumallick, L.; Elmore, B.; Hooper, A. B.; Solomon, E. I. Unpublished results.

(81) The orientation of the S(Cys)−C bond relative to the NNS plane affects the orientation of the histidine imidazole rings, due to steric reasons, leading to differences in the orientation of the histidine imidazole rings in red copper relative to blue copper.

(82) Moir, J. W. B. *Biochim. Biophys. Acta* **1999**, *1430*, 65−72.

(83) Mayburd, A. L.; Kassner, R. J. *Biochemistry* **2002**, *41*, 11582−11591.